Dalton Transactions

Accepted Manuscript

ROYAL SOCIETY OF CHEMISTRY

www.rsc.org/dalton

Dalton Transactions

RSCPublishing

ARTICLE

Localized Nano-Solid-Solution Induced by Cu Doping in ZnS for Efficient Solar Hydrogen Generation

Cite this: DOI: 10.1039/xoxxoooooox

Naixu Li[a], Longzhou Zhang[b], Jiancheng Zhou[a,]*, Dengwei Jing[b,]* and Yueming Sun[a]

Received ooth January 2012,
Accepted ooth January 2012

DOI: 10.1039/xoxxoooooox

www.rsc.org/

Nanosized photocatalysts have been shown to be important to many modern photocatalytic reactions. Control of the microstructure of the nanocrystals enables regulation of their optical properties and enhancement of specific reactions. Here, Cu^{2+}-doped ZnS nanosphere photocatalysts with hierarchical nanostructures and controllable sizes were synthesized via a facile wet-chemical reaction. We demonstrated that small amounts of Cu^{2+} doping could give rise to the formation of a variety of localized, nanosized $Cu_{1-x}Zn_xS$ solid solutions that are separated by a continuous ZnS medium. The nano-solid-solutions have predictable band structures and an average size of several nanometers, which ensures facile generation of electron-hole pairs by visible light irradiation and quick migration of the photo-generated charges to the interfaces. With Ru as a cocatalyst, the as-prepared 0.5 mol % Cu^{2+}-doped ZnS nanospheres showed a high H_2 evolution rate of 1.03 mmol h^{-1}, corresponding to a quantum efficiency of 26.2% at 425 nm. A hierarchical surface structure with a large surface area is considered crucial for the increased activity. Our work not only showed that the non-toxic metal chalcogenides achieve high efficiency but also provides a new concept of localized nano-solid-solution for photocatalytic applications.

1. Introduction

Semiconductors have a wide range of fascinating properties and can be employed for many novel catalytic reactions.[1-3] From the perspective of practical applications, nanosized semiconductor crystals are attractive for use due to their high surface/volume ratios. Among various catalytic reactions, visible-light-driven photocatalytic hydrogen production from water splitting has aroused increasing interest over the past decades and is considered a potential solution to both the energy crisis and environmental contamination.[4-10]

An efficient photocatalyst should have good light absorption properties that match the solar spectrum. Additionally, photogenerated charges in the photocatalyst should be efficiently separated and then quickly transferred to the active surface sites, which requires well-fabricated microstructures both inside and at the surface of the material. To date, numerous nanosized semiconductor catalysts, including oxides, sulfides, nitrides, have been developed.[4,8,11-25] Semiconductor transition-metal chalcogenides have been extensively studied because of their luminescent and photocatalytic properties.[26-31] In particular, UV-light-responsive zinc sulfide (ZnS) has been extensively studied.[32] ZnS usually exhibits high activity for H_2 evolution, even without the assistance of noble metals.[33-36] Despite these successful demonstrations, it is still a challenge to make ZnS work effectively under visible light irradiation due to its wide band gap. Until now, CdS was the most successful material to combine with ZnS to produce high efficiency in visible-light-driven hydrogen production.[9,37-41] However, the toxicity of CdS makes it less desirable.

CuS has recently been incorporated into ZnS-based semiconductors.[26,27,34,42] Theoretically, CuS has a very narrow band gap and thus has a good visible light response; however, its conduction band is too positive to reduce H_2O. Coupling CuS with ZnS to form a solid solution, similar to that of CdS/ZnS, has been attempted. However, in contrast to CdS, the low-temperature, stable phase for CuS is hexagonal (as differed from a cubic phase for CdS and ZnS), which governs the formation of a CuS/ZnS composite rather than a $Cu_{1-x}Zn_xS$ solid solution.[20,43,44] Additionally, CuS has a higher valence band and a lower conduction band than ZnS, resulting in the generation of type I band alignment with both photogenerated electrons and holes continuously injected into CuS. As aforementioned, photo-reduction of H_2O will not occur on CuS, which results in the recombination of the photogenerated electrons and holes in CuS. In this regard, the detailed mechanism involved in the photocatalytic H_2 production over CuS/ZnS still needs to be elucidated though some possible mechanisms have been proposed.[27,42,45]

Here, using TAA as a sulfur source and template, we successfully synthesized Cu^{2+}-doped ZnS hierarchical nanospheres with controllable size *via* a wet-chemistry approach. Because of the similar ionic radii of Cu^{2+} and Zn^{2+} (0.073 nm and 0.074 nm for Cu^{2+}

and Zn^{2+}, respectively) and, more importantly, a relatively high mobility of Cu^{2+} in the nanocrystals, it is possible to embed small amounts of Cu^{2+} into a ZnS matrix; the areas where Cu^{2+} is incorporated can, therefore, be treated as a solid solution. Moreover, our XPS results indicate that these solid solutions were enriched at the surface most likely due to the fast diffusion of these Cu^{2+} ions. Significantly, due to the very small amount of Cu^{2+} introduced, all these solid solutions were surrounded by the ZnS matrix, leading to many localized regions at the surface. The formation of such localized solid solutions can undoubtedly restrict the transmission of photogenerated charges and should be essential to the improved photocatalytic activity. Moreover, with the ideal morphology containing, for example, high surface area and good crystallinity, one can further increase the activity.

2. Experiments

2.1 Chemicals and materials

Zinc nitrate hexahydrate ($Zn(NO_3)_2{\cdot}6H_2O$), copper nitrate trihydrate ($Cu(NO_3)_2{\cdot}3H_2O$), thioacetamide (TAA), ammonium hexachlororuthenate ($(NH_4)_2RuCl_6$), sodium sulfide (Na_2S), and sodium sulfite (Na_2SO_3) were used as received. The water used in all syntheses was de-ionized water with a resistivity of 18.2 MΩ·cm.

2.2 Synthesis of Cu^{2+}-doped ZnS nanospheres with hierarchical structures

In a standard procedure, $Zn(NO_3)_2$ and $Cu(NO_3)_2$ (totaling to 10 mmol), 35 mmol of TAA, and 150 mL of water were combined in a 250-mL three-neck flask. The flask was then equipped with a reflux condenser and a Teflon-coated magnetic stir bar and preheated in air at 105 °C for 1.5 h. After cooling, the products were separated by centrifugation, washed with absolute ethanol twice and distilled water three times to remove possible residual impurities, and dried in a vacuum oven at 80 °C for 5 h. The resultant products were then sampled for future characterization. Doped ZnS samples with different amounts of Cu^{2+} were named according to the form Cu-ZnS-*x*, where *x* indicates the molar concentration of Cu^{2+}. For example, Cu-ZnS-0.5 refers to 0.5 mol % Cu^{2+}-doped ZnS.

2.3 In-situ synthesis of Ru loaded Cu-ZnS-0.5 photocatalyst

Typically, 0.1 g of the as-prepared Cu-ZnS-0.5 was dispersed using a magnetic stirrer in an aqueous solution (180 mL) containing 0.35 M of Na_2S and 0.25 M of Na_2SO_3. Next, 0.1 wt % Ru was introduced by adding $(NH_4)_2RuCl_6$ into the solution. The obtained suspension was irradiated under visible light for 5 h. After the reaction, the product was separated by centrifugation, washed with deionized water several times, and dried at 80 °C for 5 h in a vacuum oven.

2.4 Photocatalytic reactions

Photocatalytic reactions of hydrogen production from water were conducted in a closed-gas system with a side irradiation Pyrex cell (using PLS-SXE300/300UV Xe lamp irradiation) at 35 °C. The photocatalyst powder was dispersed using a magnetic stirrer in an aqueous solution (180 mL) containing Na_2S (0.35 M) and Na_2SO_3 (0.25 M) as electron donors. The photocatalysts were irradiated with visible light ($\lambda \geq 430$ nm) through a cut-off filter from the Xe lamp. The intensity and number of photons of the two light sources were measured by a fiber optic spectrometer. The amount of H_2 gas was determined using an online thermal conductivity detector (TCD) gas chromatography (NaX zeolite column, TCD detector, N_2 carrier) or drainage. Apparent quantum yields (AQY), which are defined by equation (1), were measured using a 425 nm band pass filter and an irradiation-meter. The control experiments (including without using photocatalysts/sacrificial reagents, and using Ru-ZnS photocatalysts) showed that no H_2 was produced by visible light irradiation.

$$AQY = \frac{\text{The number of reacted electrons}}{\text{The number of incident photons}} = \frac{\text{The number of evolved } H_2 \text{ molecules X 2}}{\text{The number of incident photons}} \quad (1)$$

2.5 Characterizations

X-ray diffraction (XRD) patterns of prepared photocatalysts were confirmed by an X'Pert PRO diffractometer using Cu Kα (λ=0.1538 nm) irradiation with constant instrument parameters, and all the samples were scanned between 10° and 90° with a step size of 0.033°. Diffuse reflectance UV-visible (UV-vis) spectra were measured on a Hitachi U-4100 spectrometer equipped with a lab-sphere diffuse reflectance accessory. The analysis of photoluminescence spectra (PL) was carried out at room temperature using a PTI QM-4 fluorescence spectrophotometer. The crystallite morphologic micrographs were collected using a JEOL JSM-7800F field emission scanning electron microscopy (SEM) and a FEI Tecnai G2 F30 transmission electron microscope (TEM). The X-ray photoelectron spectroscopy (XPS) measurements were conducted on an Axis Ultra, Kratos (UK) multifunctional spectrometer using monochromatic Al Kα radiation.

3. Results and Discussions

3.1 Characterizations of Cu-ZnS nanospheres

Cu^{2+}-doped ZnS (Cu-ZnS) nanocrystals were prepared by adding thioacetamide (TAA) into an aqueous solution containing $Zn(NO_3)_2$ and $Cu(NO_3)_2$. The shape evolution of Cu^{2+}-doped ZnS was monitored by changing the amount of Cu^{2+}. Figure 1 shows the representative scanning electron microscopy (SEM) images of the as-prepared Cu-ZnS nanocrystals. The samples are composed of a large quantity of well-dispersed spherical nanoparticles in terms of both size and shape. The average size of these samples, statistically estimated from the SEM images, are *ca.* 154.3 nm, 93.5 nm, 104.2 nm, 126.1 nm, 152.0 nm, and 261.2 nm for ZnS, 0 mol % Cu^{2+} (Cu-ZnS-0.1), 0.3 mol % Cu^{2+} (Cu-ZnS-0.3), 0.5 mol % Cu^{2+} (Cu-ZnS-0.5), 0.7 mol % Cu^{2+} (Cu-ZnS-0.7), and 1 mol % Cu^{2+} (Cu-ZnS-1) doped ZnS, respectively. A close examination using high-resolution SEM (insets of Figure 1) shows that these nanospheres are in fact enclosed by rough surfaces. More importantly, the surface of ZnS is smoother than the Cu^{2+}-doped ZnS, which can be seen from the valley-like structures indicated by the white arrows shown in the insets of Figure 1. To certify the existence of Cu^{2+}, Cu-ZnS-0.5 was then measured using energy dispersive X-ray spectrometry (EDX) analysis. Figure 2 shows the low-magnification SEM and the corresponding EDX mapping of the sample. Clearly, Cu^{2+} is highly dispersed in ZnS.

XRD, diffuse reflectance UV-vis absorption, and TEM were then employed to further determine the physical properties and nanostructures of these nanocrystals. As shown in Figure 3a, all of these nanospheres, including ZnS, were dominated by the cubic phase. There is no significant difference in the shape of these XRD

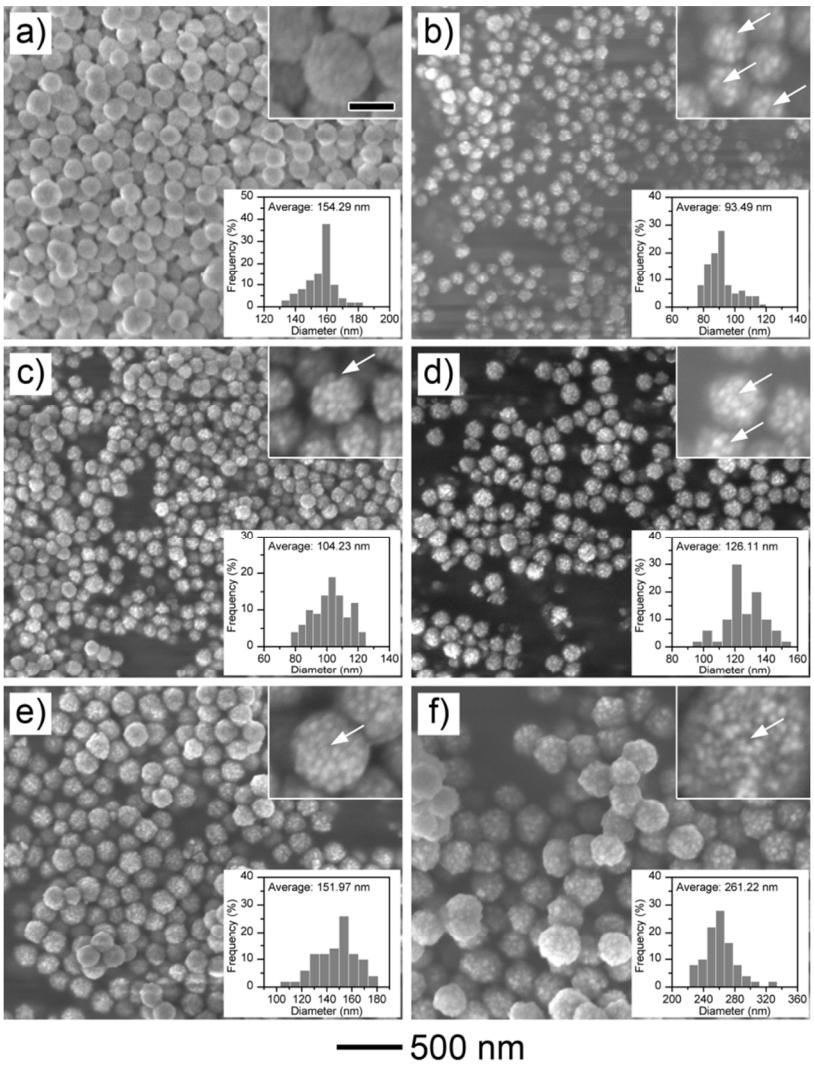

Figure 1. SEM images of different amounts of Cu^{2+}-doped into ZnS nanospheres: a) 0 mol %, b) 0.1 mol %, c) 0.3 mol %, d) 0.5 mol %, e) 0.7 mol % and f) 1 mol %. Insets are the corresponding magnified SEM images and statistical size distributions of the samples. Scale bar in the inset of a) is 100 nm and can be applied to all the other insets.

patterns, probably due to the very small amount of Cu^{2+} integrated in the ZnS substrate. Figure 3b represents the UV-vis spectra of different Cu^{2+}-doped ZnS nanospheres. A sharp absorption curve with an onset at approximately 350 nm was found in all samples, which apparently arises from a ZnS band-band electron transition.[37] Significantly, owing to the relatively high mobility of Cu^{2+}, as well as the similar ionic radii (0.073 nm and 0.074 nm for Cu^{2+} and Zn^{2+}, respectively), some Cu^{2+} ions may embed into the ZnS matrix by either replacing the Zn^{2+} or as an interstitial atom, leading to the formation of a $Cu_{1-x}Zn_xS$ solid solution (Figure 4).[27,46-52] The absorption between approximately 350 and 480 nm should therefore be a result of the formation of the $Cu_{1-x}Zn_xS$ solid solution.[42] Such a solid solution, which has variable absorption edges as marked by a red circle in Figure 3b, gives rise to a visible light response, resulting in visible-light-generated charges. Moreover, the continuously elevated absorption with the increasing Cu^{2+} throughout visible light region (> 500 nm) should be a result of the formation of CuS or non-stoichiometic $Cu_{2-x}S$ [26,42,53-55] To analyze the nanostructures of these samples, high-resolution TEM (HRTEM) measurements were then

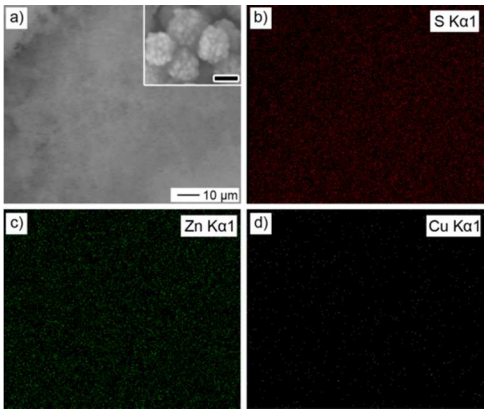

Figure 2. a) Microscaled SEM image, and b-d) the corresponding EDX mapping of Cu-ZnS-0.5 photocatalyst at the region shown in a). Scale bar in the inset of a) is 100 nm.

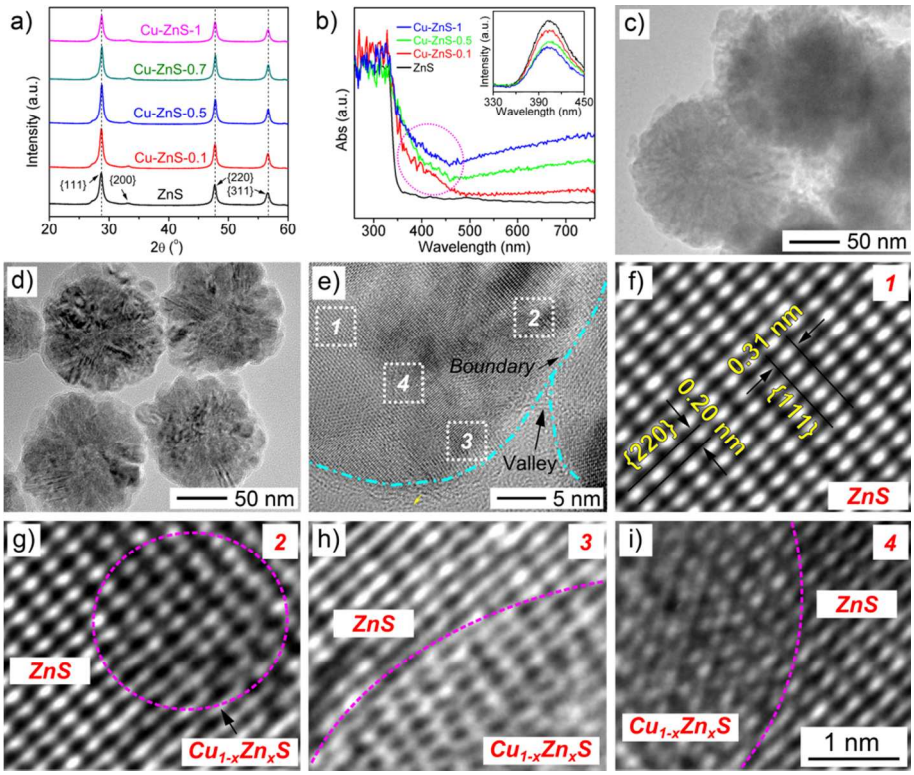

Figure 3. a) XRD patterns and b) UV-vis spectra of the as-prepared Cu^{2+}-doped ZnS nanospheres. c) and d) TEM images of ZnS and Cu-ZnS-0.3 nanospheres, respectively. e) HRTEM image of a single Cu-ZnS-0.3 nanosphere to show the size of the valley-like structure. f-i) the corresponding magnified HRTEM images shown in e) to reveal the formation of localized solid solution. Inset in b) is the PL spectra of the different amounts of Cu^{2+}-doped ZnS samples. Scale bar in i) can be applied to f-h).

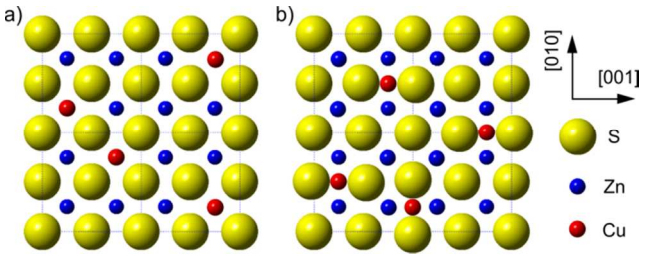

Figure 4. Schematics of the formation of $Cu_{1-x}Zn_xS$ solid solution in the form of a) substitutional solid solution and b) interstitial solid solution by replacing Zn^{2+} ions with Cu^{2+} ions or embedding Cu^{2+} in the ZnS interstitial positions. The atomic models are viewed from [100] direction.

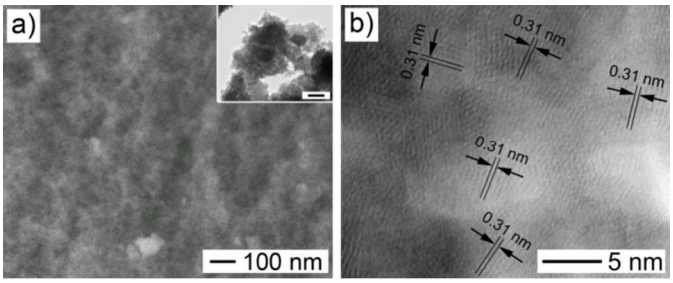

Figure 5. a) SEM and b) HRTEM images of ZnS nanocrystal obtained use Na2S instead of TAA. Inset in a) is the corresponding TEM image with lower magnification. Scale bar in the inset of a) is 50 nm.

conducted. For simplification, we chose ZnS and Cu-ZnS-0.3 as representative samples. The spherical morphology of these samples is also clearly visible. In particular, TEM images again showed the rougher surface of Cu-Zn-0.3 than that of ZnS. By carefully checking the TEM images, we notice that these nanospheres are actually aggregates of many small nanoparticles. Figure 3d shows an HRTEM image at the edge of a nanosphere in the Cu-Zn-0.3 sample. The valley-like structure is more clearly observed with a depth of *ca.* 5-10 nm between two cross-linked primary particles (Figure 3e). Moreover, as we magnified the region shown in Figure 3e, *1*, *2*, *3*, and *4* (Figure 3, f-i), we note that the regions shown in Figure 3d, in fact, contain phase segregations. For example, as shown in Figure 3f (Figure 3e, *1*), the crossed lattices with distances of 0.2 nm and 0.31 nm can be assigned to the {220} and {111} facets of pure cubic ZnS. On the contrary, when we checked the other areas indicated in Figure 3e, *2*, *3*, and *4*, significant changes in lattice configurations occurred around the adjacent ZnS matrix. The lattice distortion generated from either the substitution of Zn^{2+} by Cu^{2+} (Figure 3, g and h) or the insertion of interstitial Cu^{2+} in the ZnS matrix (Figure 3i), indicates the formation of localized $Cu_{1-x}Zn_xS$ solid solutions. In particular, the spatial separation of these localized solid solutions by the ZnS matrix results in the localized light absorption and, therefore, the confinement of the charge transmission, which contributes to an enhancement in the photocatalytic activity. These

observations again verified our UV-vis analysis that concluded the involvement of the $Cu_{1-x}Zn_xS$ solid solutions in the nanospheres. The inset in Figure 3b shows the photoluminescent (PL) properties of these samples. Significantly, the intensity gradually decreased with an increase in Cu^{2+}, which provided another indication of the incorporation of CuS and ZnS.[56]

3.2 The mechanism of formation of the Cu-ZnS nanospheres

We also examined the effects of TAA on the formation of the nanospheres. We found that TAA not only served as a sulfur source but also contributed to the ordered assembly of the initially formed nanoparticles. As shown in Figure 5, when Na_2S was used instead of TAA as a sulfur source in the synthesis of ZnS, the initially generated nanoparticles tend to rapidly aggregate in a random manner, giving rise to the formation of irregular agglomerates. This finding indicates that the initially formed primary particles tend to assemble into aggregates driven by the high surface energy.[57-59] Generally, spherical shapes have relatively low surface energy. However, without TAA, aggregation may become random, leading to the formation of large agglomerates. In fact, the TAA molecule (even after it has decomposed) has a strong bonding effect on nanoparticles arising from its terminal nitrogen, which should be responsible for the ordered assembly of the primary nanoparticles.[60-65]

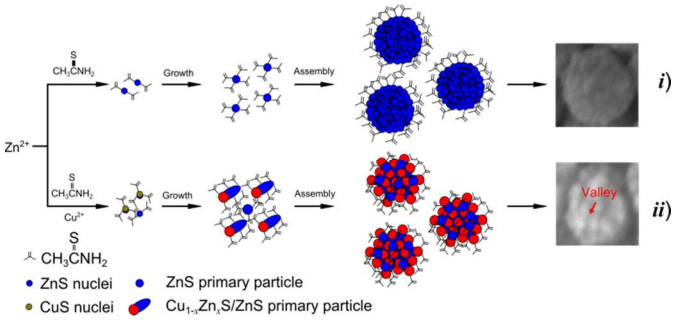

Figure 6. Plausible self-assembly process involved in the formation of i) ZnS and ii) Cu2+-doped ZnS nanospheres.

From the TEM and SEM images, Cu^{2+} was found to strongly influence the size and surface structure of the nanospheres. In fact, CuS has a much smaller solubility product than ZnS (K_{sp}: 6×10^{-37} for CuS and 2.2×10^{-22} for ZnS).[66,67] As a result, CuS should precipitate first and serve as the seeds for the growth of ZnS by forming the primary nanoparticles. In this case, the primary particle size was controlled by the concentration of Cu^{2+}, which influenced the number of CuS nucleation events. The limited number of nuclei induced by Cu^{2+}, in principle, increased the size of the primary nanoparticles. The size of the Cu-ZnS nanospheres therefore decreased due to the reduced surface energy of the primary nanoparticles. Moreover, the enlarged size of the primary particles also gave rise to the formation of many valley-structures on the surface of the nanospheres. Consequently, it is reasonable to assume that the smooth surfaces of the ZnS nanospheres were the result of the assembly of smaller ZnS primary particles. The growth mechanism of ZnS and Cu-ZnS nanospheres was thus proposed and summarized in Figure 6. Briefly, for ZnS, the growth starts from the uniformly synthesized ZnS nuclei to form the primary nanoparticles. These primary nanoparticles then assemble into nanospheres in a precise way in the presence of TAA (Figure 6, *i*). On the contrary, in the presence of Cu^{2+}, CuS instead of ZnS will form the nanoparticle seeds, followed by the growth of ZnS to form Cu-ZnS primary nanoparticles. The assembly of these primary nanoparticles then occurs (Figure 6, *ii*). Notably, the size of the nanospheres is strongly dependent on the concentration of Cu^{2+}, as it influences the number of the nuclei and therefore the size of the primary nanoparticles.

3.3 Chemical state of Cu-ZnS nanospheres

To further evaluate the surface chemical composition and electronic states of the Cu-ZnS-0.5 nanospheres, X-ray photoelectron spectroscopy (XPS) analysis was carried out. Figure 7 shows high-resolution XPS spectra of the S 2p, Zn 2p, N 1s, and Cu 2p regions. The peak centered at 161.3 eV of the S 2p shown in Figure 7a typically originates from ZnS.[26,68] A shoulder at approximately 162.1 eV was more obvious in the Cu-ZnS sample. The slight shift to higher energy might arise from the doped Cu^{2+}, which has a larger electronegativity (Cu versus Zn: 1.9 versus 1.6, Pauling scale). Similar arguments can be applied to the slight, high-energy shift in the binding energy of the Zn 2p. No significant difference in either the intensity or the peak positions of Zn and N was observed after Cu^{2+} doping, indicating that Cu^{2+} had little influence on the valence state of ZnS (Figure 7, b and c). On the other hand, the observation of N in both ZnS and Cu-ZnS again verified our hypothesis about the capping (bonding) effect of TAA (or its decomposition products). The scan over the Cu 2p region (Figure 7d) shows four peaks for Cu, i.e., 962.9 nm, 953.1 nm, 943.4 nm, and 933.17 nm. The two stronger peaks at 953.1 nm and 933.17 nm correspond to the oxidation state of Cu(II), while the rest can be assigned to satellite peaks.[26,27,69] The inset of Figure 7a shows the survey spectrum, confirming the existence of S, Zn, N, and Cu. The peaks for O and C should be attributed to air exposure of the sample and therefore the absorption of gaseous molecules, e.g., H_2O, O_2, and CO_2. The confirmation of the existence Cu^{2+} and the further observation of a slight oxidation state change for the S 2p indicate that the Cu^{2+} is embedded in the ZnS matrix. Nevertheless, when we measured the concentration of Cu^{2+} at the surface, nearly 2.2 mol % Cu^{2+} was observed. This value is much higher than the amount originally introduced (0.5%), which may be because of the fast diffusion of Cu^{2+} from the core to surface through an ion-exchange process. In particular, the diffusion is crucial to the formation of the localized $Cu_{1-x}Zn_xS$ solid solution.

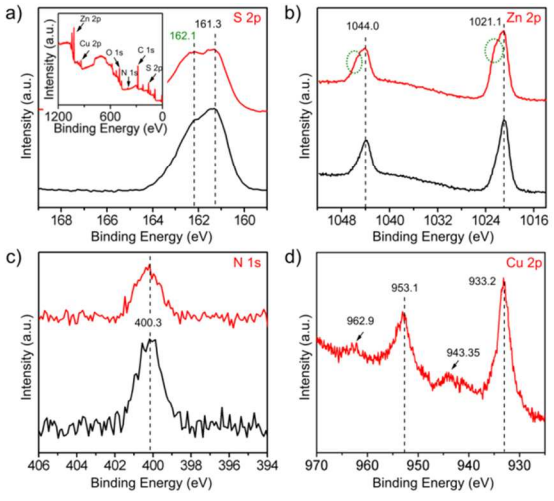

Figure 7. a-d) High-resolution XPS spectra of S, Zn, N, and Cu. The inset in a) is the survey spectrum.

3.4 Photocatalytic application

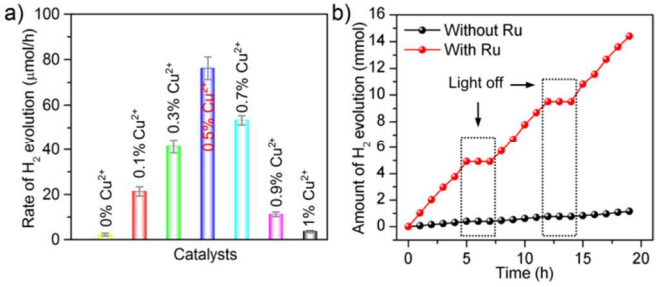

Figure 8. Photocatalytic performances of these as-prepared Cu^{2+}-doped ZnS nanospheres. a) The initial H_2 evolution rate over the different amount of Cu^{2+}-doped ZnS samples. b) Time-correlated H_2 evolutions over Cu-ZnS-0.5 (black) and 0.1 wt % Ru loaded Cu-ZnS-0.5 (red) photocatalysts.

ZnS and Cu-ZnS nanospheres were then used as catalysts in visible-light-driven hydrogen production from water. In a standard test, 0.1 g of photocatalyst was dispersed into an aqueous solution containing 0.35 M S^{2-} and 0.25 M SO_3^{2-}, followed by irradiation with visible light ($\lambda \geq 425$ nm). The gaseous products (a mixture of H_2 and N_2) were sampled from the reaction and were analyzed using a gas chromatograph. Figure 8a presents the hydrogen evolution rate calculated from a 5-hour test. A clear normal distribution of the rate over the amount of Cu^{2+}-doped in ZnS was recorded. In particular, little H_2 was measured on both the pure ZnS and the Cu-ZnS-1 samples. Cu-ZnS-0.5 exhibits the highest H_2 evolution rate, reaching 74 μmol h^{-1}. The changes in photocatalytic activity with varying concentration of doped Cu^{2+} indicates a balance in terms of both the surface area and the distribution of localized $Cd_{1-x}Zn_xS$ solid solution, *i.e.*, amount and band structures, which controls the visible-light absorption ability and the charge transmission behavior, is therefore the key contributor to the photocatalytic activity. Time-correlated H_2 evolution was then carried out the Cu-ZnS-0.5 photocatalyst to investigate its stability (Figure 8b). In the experiment, 0.1 wt % Ru was also introduced as a cocatalyst by in situ photodeposition to further increase the photocatalytic activity of the sample. Both samples presented good stability without a notable decrease in H_2 evolution. H_2 evolution over 0.1 wt % Ru loaded Cu-ZnS-0.5 photocatalyst reached 1.03 mmol/h, with a remarkable quantum efficiency of 26.2%. The steady H_2 concentration in the absence of light demonstrated that the reactions were indeed photocatalytic (see dashed rectangles in Figure 8b). According to the above analysis, the localized $Cu_{1-x}Zn_xS$ solid solution served as the active sites for visible light absorption, leading to enhanced photocatalytic performance because neither ZnS nor CuS can perform the photocatalytic reduction of H^+ in the reaction solution. The change in the concentration of doped Cu^{2+} in ZnS can affect the composition of the $Cu_{1-x}Zn_xS$ solid solution and, subsequently, the band positions, which has also been verified by the UV-vis and PL spectra.[68] On the other hand, the concentration of Cu^{2+} can significantly influence the density of the surface localized solid solution. With very small amounts of Cu^{2+} doping, there will be very few active sites available to conduct a photocatalytic reaction. On the contrary, higher Cu^{2+} doping reduces the surface area, resulting in contact of these solid solutions, leading to the continuous loss of confinement of the photogenerated charges by the localized regions, and thereby decreased photocatalytic activity. Consequently, a moderate doping level can balance both aspects, giving rise to the enhancement of photoactivity and the normal variation of the photocatalytic activity relative to different Cu^{2+}-doped ZnS samples. It is also worth pointing out that, if large amount Cu^{2+} are introduced, CuS, instead of the solid solution, emerges as the dominate product. As we mentioned, the fate of photogenerated electrons in the conduction band of CuS will be recombination with photogenerated holes; excessive doping of Cu^{2+} should be avoided. The mechanism for the entire photocatalytic reaction, based on the irradiation of localized $Cd_{1-x}Zn_xS$ nano-solid-solutions (Figure 9a), was proposed in Figure 9. Briefly, as shown in Figure 9, b and c, upon excitation of the solid-solution segments by visible light, the photogenerated electrons and holes are confined and accumulated at active sites, leading to fast oxidation and reduction reactions. The presence of noble-metal cocatalysts improves the spatial separation of the electrons and holes, leading to a further acceleration of the reduction of H^+ into H_2.[71-72] More importantly, the hierarchical spherical morphology with numerous valley-like structures guarantees a high density of surface localized solid solutions, *i.e.*, the active sites, which is an indispensable factor for high photocatalytic activity.

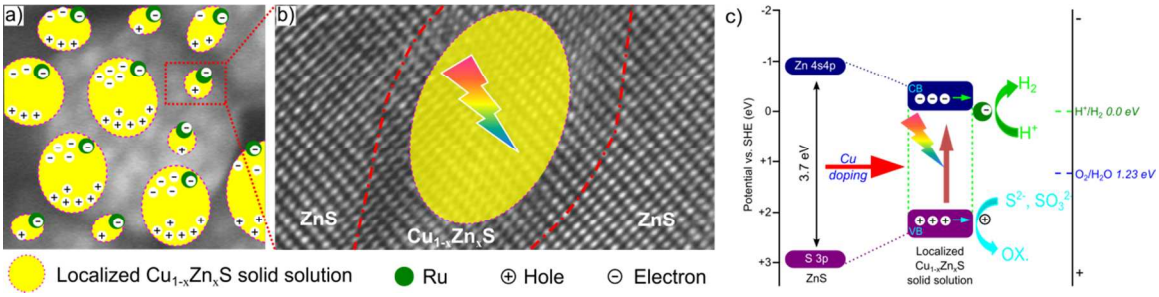

Figure 9. Plausible mechanism involved in the visible-light-driven H_2 evolution process over an as-prepared, Cu^{2+}-doped ZnS nanosphere. a) Formation of many nanosized localized $Cu_{1-x}Zn_xS$ solid solutions separated by ZnS medium. b) Magnification over a typical $Cu_{1-x}Zn_xS$ solid solution surrounded by ZnS. c) Proposed band edges of Cu doping localized solid solution for solar hydrogen generation.

Conclusions

In summary, Cu^{2+}-doped ZnS nanospheres with controllable sizes and hierarchical structures were prepared using a facile wet-chemical method. These nanospheres doped with different amount of Cu^{2+} showed a predictable visible light response. Efficient visible-light-driven hydrogen production over a 0.5 mol % Cu^{2+} photocatalyst was achieved, with an initial H_2 evolution rate of 1.03 mmol/h and a remarkably high quantum efficiency of 26.2%. It is assumed that a small amount of Cu^{2+} doping allows these Cu^{2+} ions to easily embed into the ZnS matrix, leading to the formation of islands of localized $Cu_{1-x}Zn_xS$ solid solutions with sizes well below 5 nm. Charges can

be easily generated by visible light irradiation and can quickly migrate to the active surface sites of the photocatalyst. These localized $Cu_{1-x}Zn_xS$ solid solutions served as the active centers, absorbing visible light to initiate the photocatalytic reactions. The demonstration of doping induced localized nano-solid-solution advances our understanding of the role of a dopant on band structure engineering and provides a new insight into photocatalytic reactions in composite semiconductor catalysts.

Acknowledgements

This work was financially supported by the National Nature Science Foundation of China (No. 31070517, 21276206) and the National Basic Research Program of China (973 Program, No. 2013CB932902).

Notes and references

a School of Chemistry and Chemical Engineering, Southeast University, Nanjing, 211189, P.R. China

b International Research Center for Renewable Energy, State Key Laboratory of Multiphase Flow, Xi'an Jiaotong University, Xi'an, Shaanxi 710049, P. R. China

*Corresponding author. E-mail: jczhou@seu.edu.cn (Prof. J. Zhou) and dwjing@mail.xjtu.edu.cn (Prof. D. Jing)

1 Y. Xia, Y. Xiong, B. Lim, S. E. Skrabalak, *Angew. Chem. Int. Ed.,* 2009, **48**, 60-103.
2 M. R. Hoffmann, S. T. Martin, W. Choi, D. W. Bahnemann, *Chem. Rev.*, 1995, **95**, 69-96.
3 H. Tong, S. Ouyang, Y. Bi, N. Umezawa, M. Oshikiri, J. Ye, *Adv. Mater*., 2012, **24**, 229-251.
4 A. Fujishima, K. Honda, *Nature*, 1972, **238**, 37-38.
5 M. Gratzel, *Nature*, 2001,**414**, 338-344.
6 Q. Li, B. Guo, J. Yu, J. Ran, B. Zhang, H. Yan, J. R. Gong, *J. Am. Chem. Soc.*, 2011,**133**, 10878-10884.
7 X. Chen, S. Shen, L. Guo, S. S. Mao, *Chem. Rev.*, 2010, **110**, 6503-6570.
8 X. Wang, K. Maeda, A. Thomas, K. Takanabe, G. Xin, J.M. Carlsson, K. Domen, M. Antonietti, *Nat. Mater.*, 2009, **8**, 76-80.
9 M. Liu, L. Wang, G. M. Lu, X. Yao, L. Guo, *Energy Environ. Sci.,* 2011, **4**, 1372-1378.
10 X. Chen, C. Li, M. Gratzel, R. Kostecki, S.S. Mao, *Chem. Soc. Rev.*, 2012, **41**, 7909-7937.
11 Z. Zou, J. Ye, K. Sayama, H. Arakawa, *Nature*, 2001, **414**, 625-627.
12 K. Maeda, K. Teramura, D. Lu, T. Takata, N. Saito, Y. Inoue, K. Domen, *Nature*, 2006, **440**, 295.
13 X. Chen, L. Liu, P. Y. Yu, S. S. Mao, *Science*, 2011, **331**, 746-750.
14 Z. Li, W. Luo, M. Zhang, J. Feng, Z. Zou, *Energy Environ. Sci.*, 2013, **6**, 347-370.
15 L. G. Devi, R. Kavitha, *Appl. Catal. B-Environ*., 2013, **140-141**, 559-587.
16 Y. Liu, J. Hu, C. Ngo, S. Prikhodko, S. Kodambaka, J. Li, R. Richards, *Appl. Catal. B-Environ.,* 2011, **106**, 212-219.
17 N. Bao, L. Shen, T. Takata, K. Domen, *Chem. Mater.*, 2007, **20**, 110-117.
18 Z. Lei, W. You, M. Liu, G. Zhou, T. Takata, M. Hara, K. Domen, C. Li, *Chem. Commun.*, 2003, **17**, 2142-2143.
19 H. Labiadh, T. B. Chaabane, L. Balan, N. Becheik, S. Corbel, G. Medjahdi, R. Schneider, *Appl. Catal. B-Environ.*, 2014, **144**, 29-35.
20 D. Jing, L. Guo, *J. Phys. Chem.*, 2006, **110**, 11139-11145.
21 H. Ma, J. Han, Y. Fu, Y. Song, C. Yu, X. Dong, *Appl. Catal. B-Environ.*, 2011, **102**, 417-423.
22 H. Kato, K. Asakura, A. Kudo, *J. Am. Chem. Soc.*, 2003, **125**, 3082-3089.
23 Y. Hou, F. Zuo, A. Dagg, P. Feng, *Nano Lett.*, 2012, **12**, 6464-6473.
24 X. Yang, H. Cui, Y. Li, J. Qin, R. Zhang, H. Tang, *ACS Catal.*, 2013, **3**, 363-369.
25 A. Mukherji, R. Marschall, A. Tanksale, C. Sun, S. C. Smith, G. Q. Lu, L. Wang, *Adv. Funct. Mater.*, 2011, **21**, 126-132.
26 J. Yu, J. Zhang, S. Liu, *J. Phys. Chem. C*, 2010, **114**, 13642-13649.
27 J. Zhang, J. Yu, Y. Zhang, Q. Li, J. R. Gong, *Nano Lett.*, 2011, **11**, 4774-4779.
28 F. Gu, C. Z. Li, S. F. Wang, M.K. Lü, *Langmuir*, 2005, **22**, 1329-1332.
29 I. Tsuji, H. Kato, A. Kudo, *Angew. Chem. Int. Ed.*, 2005, **44**, 3565-3568.
30 Y. Li, G. Chen, C. Zhou, J. Sun, *Chem. Commun.*, 2009, **15**, 2020-2022.
31 M. Antoniadou, V. M. Daskalaki, N. Balis, D.I. Kondarides, C. Kordulis, P. Lianos, *Appl. Catal. B-Environ.*, 2011, **107**, 188-196.
32 T. Mandal, P. K. Maiti, C. Dasgupta, *Phys. Rev. B*, 2012, **86**, 024101.
33 J. F. Reber, K. Meier, *J. Phys. Chem.*, 1984, **88**, 5903-5913.
34 H. Youn, S. Baral, J. H. Fendler, *J. Phys. Chem.*, 1988, **92**, 6320-6327.
35 D. NeiláFurlong, J. Chem. Soc., *Faraday Trans.*, 1990, **86**, 3637-3640.
36 N. Zeug, J. Bücheler, H. Kisch, *J. Am. Chem. Soc.*, 1985, **107**, 1459-1465.
37 C. M. Huang, S.H. Cheng, U.S. Jeng, C.S. Yang, L. W. Lo, *Nano Res.*, 2012, **5**, 654-666.
38 S. K. Maji, A.K. Dutta, S. Dutta, D. N. Srivastava, P. Paul, A. Mondal, B. Adhikary, *Appl. Catal. B-Environ.*, 2012, **126**, 265-274.
39 J. A. Villoria, R. M. Navarro Yerga, S. M. Al-Zahrani, J. L. G. Fierro, *Ind. Eng. Chem. Res.*, 2010, **49**, 6854-6861.
40 J. Zhang, J. Yu, M. Jaroniec, J. R. Gong, *Nano Lett.*, 2012, **12**, 4584-4589.
41 M. Liu, D. Jing, Z. Zhou, L. Guo, *Nat. Commun.*, 2013, **4**, 2278.
42 A. Kudo, M. Sekizawa, *Catal. Lett.*, 1999, **58**, 241-243.
43 J. Yu, J. Zhang, M. Jaroniec, *Green Chem.*, 2010, **12**, 1611-1614.
44 Y. Liu, D. Qin, L. Wang, Y. Cao, *Mater. Chem. Phys.*, 2007, **102**, 201-206.
45 T. Arai, S. Senda, Y. Sato, H. Takahashi, K. Shinoda, B. Jeyadevan, K. Tohji, *Chem. Mater.*, 2008, **20**, 1997-2000.
46 M. Schindler, F. C. Hawthorne, *J. Solid State Chem.*, 1999, **146**, 271-276.
47 R. Shannon, *Acta Crystallogr. A*, 1976, **32**, 751-767.
48 W. G. Zeier, A. LaLonde, Z. M. Gibbs, C.P. Heinrich, M. Pantho□fer, G. J. Snyder, W. Tremel, *J. Am. Chem. Soc.*, 2012, **134**, 7147-7154.
49 M. Belaïche, M. Bakhache, M. Drillon, A. Derory, *Chem. Phys. Lett.*, 2004, **394**, 147-149.
50 S. Hou, X. Zhang, H. Mao, J. Wang, Z. Zhu, W. Jing, *Phys. status solidi B*, 2009, **246**, 2333-2336.
51 P. Yang, C. Song, M. Lü, G. Zhou, Z. Yang, D. Xu, D. Yuan, *J. Phys. Chem. Solids*, 2002, **63**, 639-643.

52 M. Kuppayee, G. K. Vanathi Nachiyar, V. Ramasamy, *Appl. Surf. Sci.*, 2011, **257**, 6779-6786.
53 X. Wang, C. Xu, Z. Zhang, *Mater. Lett.*, 2006, **60**, 345-348.
54 Y. Zhao, H. Pan, Y. Lou, X. Qiu, J. Zhu, C. Burda, *J. Am. Chem. Soc.*, 2009, **131**, 4253-4261.
55 Y. Zhao, C. Burda, *Energy Environ. Sci.*, 2012, **5**, 5564-5576.
56 W. Q. Peng, G. W. Cong, S. C. Qu, Z. G. Wang, *Opt. Mater.*, 2006, **29**, 313-317.
57 Y. Li, X. He, M. Cao, *Mater. Res. Bull.*, 2008, **43**, 3100-3110.
58 Y. Luo, G. Duan, M. Ye, Y. Zhang, G. Li, *J. Phys. Chem. C*, 2008, **112**, 2349-2352.
59 J. S. Hu, L.L. Ren, Y. G. Guo, H. P. Liang, A. M. Cao, L. J. Wan, C. L. Bai, *Angew. Chem. Int. Ed.*, 2005, **44**, 1269-1273.
60 H. Tong, Y.-J. Zhu, L.-X. Yang, L. Li, L. Zhang, *Angew. Chem. Int. Ed.*, 2006, **45**, 7739-7742.
61 L. Mi, Q. Ding, H. Sun, W. Chen, Y. Zhang, C. Liu, H. Hou, Z. Zheng, C. Shen, *CrystEngComm*, 2013, **15**, 2624-2630.
62 Q. Hu, G. Tong, W. Wu, F. Liu, H. Qian, D. Hong, *CrystEngComm*, 2013, **15**, 1314-1323.
63 Y.-J. Hsu, S.-Y. Lu, Y.-F. Lin, *Chem. Mater.*, 2008, **20**, 2854-2856.
64 R. Jin, G. Chen, Q. Wang, J. Sun, Y. Wang, *J. Mater. Chem.,* 2011, **21**, 6628-6635.
65 R. Jin, G. Chen, J. Pei, H. Xu, Z. S. Lv, *RSC Adv.*, 2012, **2**, 1450-1456.
66 J. A. Dean, Lange's handbook of chemistry, McGraw-Hill, New York, 1998.
67 F. Huang, Y. Lan, P. Chen, *J. Mater. Sci.,* 2011, **46**, 5732-5736.
68 J. Shan, P. Pulkkinen, U. Vainio, J. Maijala, J. Merta, H. Jiang, R. Serimaa, E. Kauppinen, H. Tenhu, *J. Mater. Chem.*, 2008, **18**, 3200-3208.
69 J. Ghijsen, L. H. Tjeng, J. Van Elp, H. Eskes, J. Westerink, G.A. Sawatzky, M.T. Czyzyk, *Phys. Rev. B*, 1988, **38**, 11322-11330.
70 R. Viswanatha, D. M. Battaglia, M.E. Curtis, T.D. Mishima, M.B. Johnson, X. Peng, *Nano Res.*, 2008, **1**, 138-144.
71 F. Lin, Y. Zhang, L. Wang, Y. Zhang, D. Wang, M. Yang, J. Yang, B. Zhang, Z. Jiang, C. Li, *Appl. Catal. B-Environ.*, 2012, **127**, 363-370.
72 H. Yu, R. Liu, X. Wang, P. Wang, J. Yu, *Appl. Catal. B-Environ.*, 2012, **111-112**, 326-333.

Graphical abstract

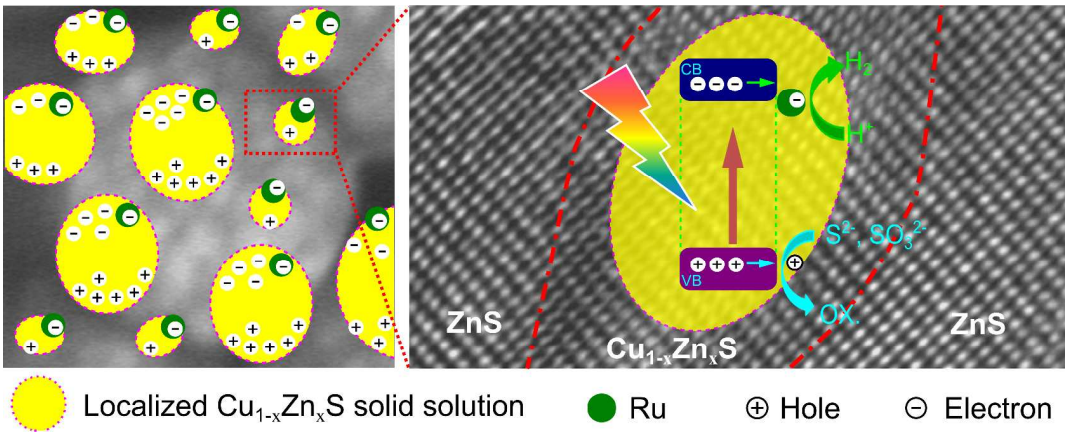

Visible-light-driven H_2 evolution rate reached 1.03 mmol/h with a quantum yield of 26.2% over the localized $Cu_{1-x}Zn_xS$ nano-solid-solutions.